KIT

Karlsruhe Institute of Technology

Muon induced secondary electrons at the KATRIN experiment
Detector installation and setup and data analysis

Diploma Thesis of

Philipp Rovedo

At the Department of Informatics
IKP - Institut fuer Kernphysik - KIT Karlsruhe

Reviewer:	Prof. Dr. Guido Drexlin
Second reviewer:	Prof. Dr. Ulrich Husemann
Advisor:	Nancy Wandkowsky
Second advisor:	?

Duration:: September 27th 2012 – September 27th 2013

I declare that I have developed and written the enclosed thesis completely by myself, and have not used sources or means without declaration in the text.

PLACE, DATE

....
    (**YOUR NAME**)

Contents

1. Introduction

1.1. Neutrinos in the standard model

During the second part of the 20th century, a model stating 16 particles has been developed to describe a huge portion of known phenomena, the standard model. It contains six quarks, six leptons (both made up of three particle generations) and four types of Gauge Bosons. The latter are carriers of the standard models interactions of the former particles, meaning all interactions of matter are based on the exchange of one or more of the Gauge Bosons. For our universe, gravity, the graviton generated force, plays a major role for formation and stability af almost all larger structures. In particle physics however, it can mostly be neglected. Here, only the strong and weak as well as the electromagnetic interaction make for noticable contributions to phenomena observed. Most of what we can observe with our bare eyes or in basic experiments is attributable to the electromagnetic force or gravity, however, strong and weak interaction do play a major role when it comes to high energy physics. Here, the limited reach of the two is overcome by small distances between interacting particles. In case of the neutrino, detection and by that the study of its characteristics is even more difficult as it interacts only gravitationally and weakly. Now, as mentioned before, gravity is indeed long range, but very weak in force. And although weak intraction is a lot stronger compared to gravity, it is still weak compared to both electromagnetic and strong interactions. That is why the neutrino is considered elusive, detection efficiencies are low and only large scale detectros are able to detect statistically relevant amounts of neutrinos. In the standard model, neutrinos are considered massless. Many experiments have shown that the weightless neutrino is a wrong assumption. Most of these were experiments prooving neutrino oscillatinos with both reactor neutrinos and solar neutrinos such as Kamiokande[Abe13] or **(add experiments)**.   **ToDo**

Up till now, only the differences of the squared masses are known. This leads to different relations depending on how masses are distributed between the flavours, 1.1, and how large they are absolutely 1.2. This problem is solved by the knowledge of one of the masses. KATRIN is on the verge of finding the ν_e's mass.[BKR09]
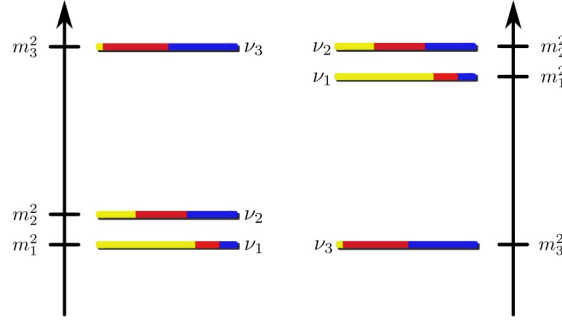
Figure 1.1.: sadf[asd12]

Figure 1.2.: asdf

1.1.1. Neutrino Oscillations

If the neutrinos were without mass, its mass eigenstates would equal its flavour eigenstates:

$$
\begin{aligned}
|\nu_e> &= |\nu_1> \\
|\nu_\mu> &= |\nu_2> \\
|\nu_\tau> &= |\nu_3>
\end{aligned}
\tag{1.1}
$$

First doubts concerning this asumptions occured as inconsistencies between the measured and the calculated solar ν-flux occured. As the counton ν_e was too low, the theory of neutrino oscillations emerged stating, that a mixture of flavours was possible as the flavours were made up of all three of the mass eigenstates. The Mixture is described by the so called Pontecorvo-Maki-Nakagawa-Sakata matrix:

$$
\begin{pmatrix} |\nu_e> \\ |\nu_\mu> \\ |\nu_\tau> \end{pmatrix} = \begin{pmatrix} \theta_{e,e} & \theta_{e,\mu} & \theta_{e,\tau} \\ \theta_{\mu,e} & \theta_{\mu,\mu} & \theta_{\mu,\tau} \\ \theta_{\tau,e} & \theta_{\tau,\mu} & \theta_{\tau,\tau} \end{pmatrix} \begin{pmatrix} |\nu_{m,e}> \\ |\nu_{m,\nu}> \\ |\nu_{m,\tau}> \end{pmatrix}
\tag{1.2}
$$

1.1.2. Direct measurement of neutrino mass

Direct measurements of the neutrino mass require a reaction known to include neutrinos in its equation. There are both spectrometric and calorimetric approaches. While the scale of spectrometers is getting bigger and bigger, calorimetric approaches seem to be a reasonable alternative, although the slow detector response - the detector material itself is decaying - requires for large arrays of detectors leading to extensive space requirements as well at some point. The luminosity of spectrometer experiments though is unachieved by any other. That is why the KATRIN collaboration is working on a setup to measure electrons from Tritium decay to determine the neutrino mass.

1.1.3. Indirect measurement of neutrino mass

Another approach is using indirect ways of finding the neutrino mass. One possibility here is to search for neutrinoless double beta decay, $0\nu\beta\beta$, which can exist only if the neutrino is its own anti-particle, a so called majorana neutrino. Then, if two nuclei beta decay, the neutrino from one vertex can be absorbed in the second as an anti-neutrino - or vice versa. The decay would then not emit any neutrino and the rate would be dependant on the "effective Majorana neutrino mass square" [DHMW13]:

$$
\Gamma_{0\nu\beta\beta} \propto \left| \sum U_{ei}^2 m\left(\nu_i\right) \right|^2
\tag{1.3}
$$

1.2. Cosmic muons and their interaction with matter

When high energy particles hit the upper parts of the atmosphere, a cascade of particles generated from the interaction with atmospheric molecules and atoms follows. Most primary particles are nucleons, most of which are free protons, meaning Hydrogen ions. Helium nucleons' fluxes are already about a order of magnitude below that, higher mass number nuclei show even lower rates[Sta04]. By different interactions

2. The KATRIN experiment

The KATRIN experiment is on its way to measure the neutrino mass or set new upper limits at precisions never achieved before. It will reach a sensitivity of $500\,\mathrm{meV/c^2}$ excelling the previously best experiments of Mainz and Troisk by a factor of **(how much?)**. Major challenges of the project are the requirement of ultra high vacuum, the exat knowledge of all magnetic and electic fields as well as external influences on those, the required high luminosity of the Tritium source and the reduction of background sources.

2.1. Measurement principle

A generally easy principle is used to find information on the neutrino mass: The energy of electrons from tritium decay is measured with high precision and compared to the standard model's presumption for a massless neutrino:

$$^3_1\mathrm{T} \longrightarrow \,^3_1\mathrm{H}^+ + \mathrm{e}^- + \bar{\nu}_e \tag{2.1}$$

As the decay's energy is distributed between the constant masses of electron end neutrino and their kinectic energies respectively, the decay electrons will show a continous spectrum. The difference between standard model's calculated electron energy and to the extrapolated maximum electron energy from the spectrum then equals the neutrino mass. A different light is shed on the easiness of the task when considering the needed accuracy of the electron's energy.

2.1.1. MAC-E Filter

A high luminousity is a major requirement for good statistics at the KATRIN experiment. This makes it impossible to use some kind of aperture to filter for electrons from Tritium decay with one momentum direction as they are emitted uniformly from the source volume and the largest amount of electrons would never reach the main spectrometer. That is why another strategy is used at KATRIN: The MAC-E filter - magnetic adiabatic collimation with electrostatic filter - utilises the fact that, under small enough magnetic field changes, the magnetic momnetum of a particle is constant and the particle is considered adiabatic.

2.2. Source Side and Transport Section

2.3. Pre-Spectrometer

The pre-spectrometer was built in Munster and works on the same principle as the main spectrometer, although being a lot smaller. It is installed to reduce the flux to the main

spectrometer, and by that the possible amount of stored electrons inside the main vessel. The pre-spectrometer has a one layered inner electrode to shield against externally induced electrons.

2.4. Main Spectrometer

2.5. Focal Plane Detector System

The main detector is located at the very north of the experiment. It is made up of a silicon wafer divided into 148 pixels all of which cover the same surface area in different shapes. Every pixel has the same surface area, making rates more easily comparable - at least in fairly homogenous magnetic fields.

2.6. Solenoids

2.7. Air coil system

3. The muon detection system

The need for low background rates at the main detector requires for a good knowledge of background sources. Despite magnetic reflection and wire electrodes, cosmic ray and particularly cosmic muon induced background may be an issue for the KATRIN experiment. To gather and asess muon related data, scintillator modules have been installed at both the monitor spectrometer and the main spectrometer. While the monitor spectrometer is equipped with only two rather small modules, at the larger main spectrometer, 8 modules have been installed at different positions enabling the user to cover different regions of the vessel. This freedom is enlarged by installing the detection system on three independently movable trolleys. The modules have been connected to the DAQ one trolley per card, meaning modules one and two connect to card three, modules 3 through 5 to card six and modules 6 through 8 to card nine (3.1) All connections from modules to DAQ are made of coaxial cabling of equal length. This ensures comparable timestamps which are assigned only after the analogue signals arrive at the DAQ. High voltage is provided by two supplies, one on the east and one on the west side of the main hall. All devices of the muon detection system are connected to two multiplugs that are both overcurrent protected and feature mains filters. These multiplugs have been modified 3.1 to connect to a ground other than the outlet's. To ensure a common potential for all of the devices and the surrounding appliances this connection was made to the trough below the main vessel.

(insert photograph of multiplug)   **ToDo**

3.1. Data aquisition crate

The Data acquisition crate, short DAQ, is the central part of event recording and by that the interface between hardware muon modules and software based ORCA machine. It

Module	1A	1B	2A	2B	3A	3B	4A	4B
Card	3	3	3	3	6	6	6	6
Channel	0	14	3	7	0	14	3	7

Module	5A	5B	6A	6B	7A	7B	8A	8B
Card	6	6	8	8	8	8	8	8
Channel	9	23	0	14	3	7	9	23

Table 3.1.: Assignment of module sides to cards and channels

Figure 3.1.: Added extension of the earthing contact to connect to any ground needed

features first and second level trigger cards that are described in detail in the following
chapters. The linux based system runs on an external hard drive connected to the second
level trigger card via USB. Here, a screen and keyboard can be connected for network
setup, then, access via ssh is possible. The DAQ can be connected to and controlled by the
ORCA software.

3.1.1. First level trigger cards

The FLT cards directly receive the signal output of the photomultiplier tubes via coaxial
cabling. They then do first parts of data analysis to reduce data flow to the ORCA machine.
In this case, only events with occur simultaneously on both sides of any module are passed
ToDo on. This reduces the rate from **(look up non veto rate)** to around 250 Hz. The FLT
cards are made up of a large main card and a smaller connector card.

3.1.2. Second level triger cards

Only one second level trigger card is installed on each DAQ. all the Signals from the FLT
cards are stacked here and passed on to the the ORCA machine. Networking runs directly
through the SLT card. Other connections, such as USB, a display port, and also the CAT
5 connectors for synchronisation to a clock can be attached here.

3.2. Orca control

ORCA is the central software for data acquisition. It is able to control lots of different
devices via almost any kind of interface, while it is easiest to use ethernet connections.

3.2.1. Software Gains and Thresholds

3.2.2. Run control

Runs are the basic element of data storage, every time data is recorded, a run is created.
Inside every run can be a number of subruns, at least there is one, that will in turn contain
data classes such as KaLi::KLVetoEvents, the most used event class in case of the muon
modules.

3.2.3. File handling

All runs created are first saved to the local disc of the Mac machine. Sorting in folders
for year and month is applied to quickly find what zou are looking for. They are then
uploaded to servers of the IPE via cronjobs, a feature of the Linux based MacOS. Using
the KaLi software, the user can then access this data from anywhere he has a fast enough
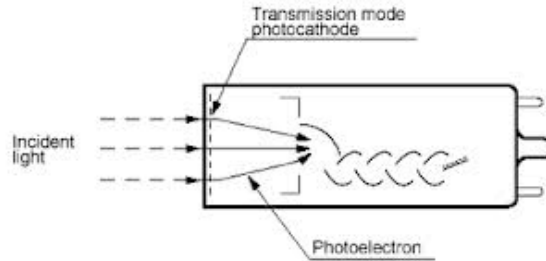internet connection.

Figure 3.2.: Schematic view of a photomultiplier tube with incident photons and photo-electrons emerging. Note the nested dynode structure for cascading purposes.

3.2.4. Orca Fit

3.3. Scintillator modules

The central part of the detection system are the eight scintillator modules. They are made of the synthetic material BC-412 which is utilized in applications requiring large area coverage [Cry05]. These have previously been used at **(From Where?)**. Every scintillator cuboid is read out by two sets of four photomultiplier tubes. Photons arriving at the short ends of the module are guided to the photomultiplier tubes via non-scintillating material which, away from that, exhibits similar optical properties. All other sides of the scintillator are covered in reflective foil to push detection efficiency to the maximum. Of the eight photomultiplier tubes per scintillator module installed, 4 are read out via one FLT channel. The background of low energy events can be reduced significantly by recording only events occuring on both sides of the module at once. Only coincident signals should be recorded by the DAQ, though, on some occasions, quite a lot of single side signals occur. To account for those, every dataset is first analysed by a search algorithm (4.2.2) to filter them.**(reference search algorithms)**

ToDo

ToDo

3.4. Photomultipliers

Each Photomultiplier tube is made up of a layer of **(of what)** where photons from scintillation ionize the layers' atoms leaving electrons with their initial Energy less the ionization energy

ToDo

$$E_{e^-} = E_{phot} - E_{ion}$$

The electron is then accellerated and guided by the electric field from dynode to dynode, cascading to more and more electrons, as each electron's energy rises by $e \cdot U_{acc}$ between each pair of dynodes.

3.5. Gains, Thresholds and Acceleration Voltages

To achieve the best possible event detection, the photomultipliers' acceleration voltages as well as the software gains and thresholds in Orca had to be adjusted. The focus here was to obtain landau peaks with equal heigt and width, as the rates throughout the modules can be considered equal over large time intervals compared to the inverse rate. At first, the acceleration voltages were kept low to limit the signal peaks' heigts to aroud $2\,\mathrm{V}$. Carefully setting the mentioned parameters, one achieved the following, well alligned curves. A problem remaining at the time though was that the electronic noise set in pretty close to the peak position, only slightly shifted to lower energies. This meant that thresholds hat to be set close to the peak bin as well, loosing low energy events in the process. **(root graph**

ToDo
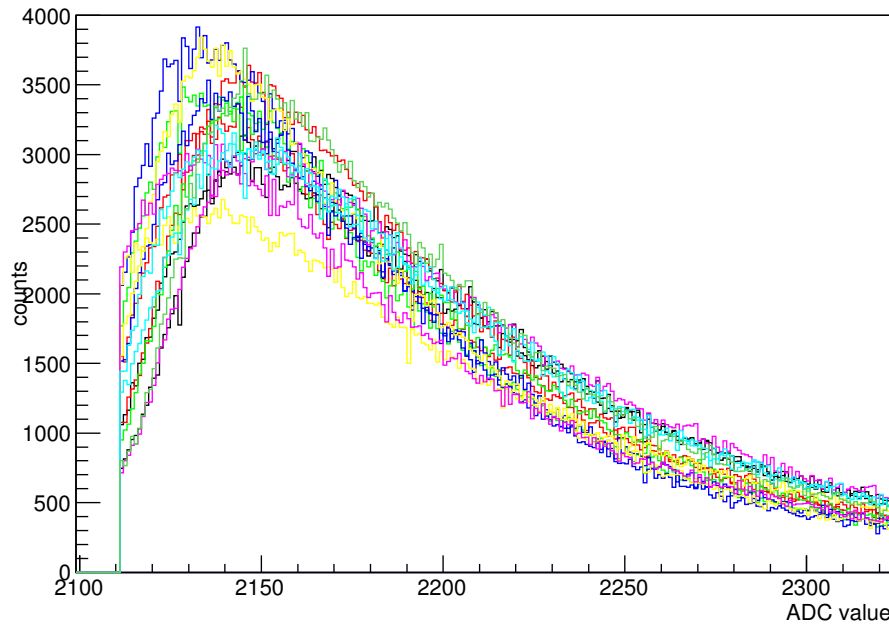
Figure 3.3.: The landau peak at acceleration voltages around 1200 V. All channels show similar width and height. Note that the threshols had to be set pretty close to the peak position as noise was a huge issue under the conditions.

instead of orca, move to commissioning measurements?)

Later in the comissioning process, it got clear from the handbooks that the photomultiplier tubes had to be operated at accelleration voltages of 1.5 kV and above. To keep the singnals' height as small as possible, most of the tubes were limited to this minimal voltage, **ToDo** wheras the sides **(which ones)** were set to 1.6 kV over showing lower rates than the others. Following this procedure, the tubes seemed much more stable and comparable, as **ToDo** all the gains and thresholds could now be set to the same values of **(enter values)** and respectively, while still showing aligned peak positions 3.4. This is a huge advance to before when gains varied by a factor of almost up to four.

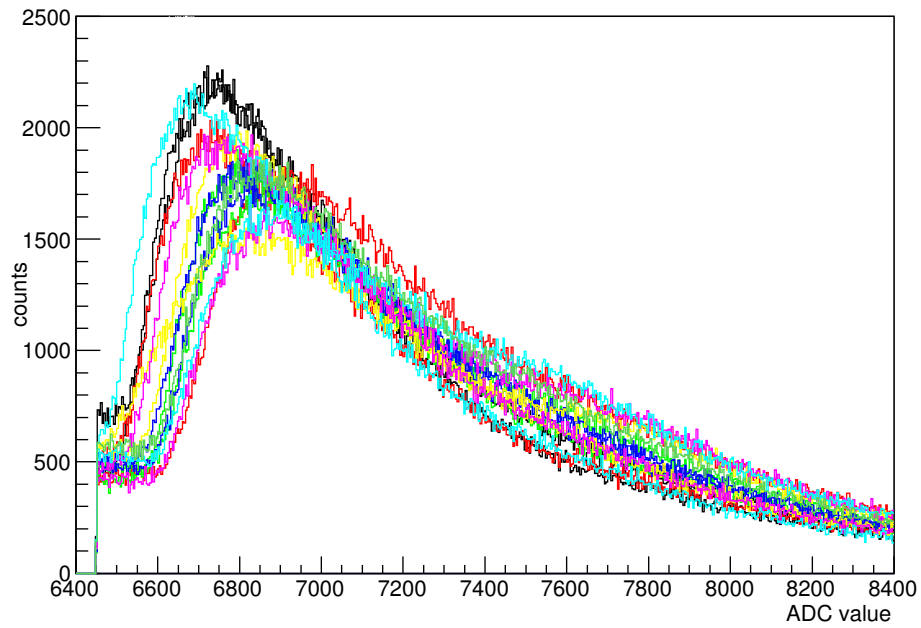Figure 3.4.: Landau peaks after raising acceleration voltages. Note that this pattern was achieved solely by raising two module's side's acceleration voltages to $1.6\,\mathrm{kV}$ leaving gains and thresholds at the same level for all channels.

4. Analysis software

To analyse the data recorded by DAQ and ORCA software, completely new data structures fit to the needs of muon detection and coincidence analysis have been created. Methods have been implemented to further investigate data stored inside those structures. A cmake file has been created making it possible to install the program on any machine used for analysis. All the sources including the main programs are available on the svn repository **(move program(s) to svn repository)**. Doing so, external programs can be modified for custom analysis that shall include muon data making it very modular. **ToDo**

4.1. Data structure

All data from the IPE-servers arrives converted from ORCA-specific formatting to .root files compatible with CERN's analysis software ROOT. Hence, ROOT Methods are used to extract data from these structures, while most of these methods are implemented as part of the KaLi package in Kasper, which constitutes for a complete and closed data transfer protocol. Through those structures, data specified by the user will be cached locally and can be analysed afterwards.// For analysis with the classes described here, all data is transfered from the cached files to runtime storage. Here, the newly written class **event** with the following members comes into play.

<div align="center">event private class members</div>

- fADCValue

- fTimeSec

- fTimeSubSec

- fPanel

- fSide

For each member, corresponding set- and get-methods have been implemented making them accessible to the programmer. Furthermore, the operators "<", "<=", ">", ">=", "==", and "-" have been overloaded to compare the timestamps of the event class. This

was useful especially since ADCValues are merely used for plausibility checking of the data but not for quantitative analysis. Doing so, events and the classes derived can easily be compared and searching becomes cleaner and clearer.

Derived from the base event class are two more storage classes:

panelEvent storing a second ADCValue

<div align="center">

coincidentEvent additional member

</div>

- fADCValue2

and the common timestamp of events activating both panel sides and **coincidentEvent** storing ADCValues of simultaneous events in multiple modules and the number of modules involved:

<div align="center">

coincidentEvent additional members

</div>

- std::vector fADCValues

- fnPanels

Every ORCA-run then utilizes the class **run** storing the data of the .root files in vectors of events. Recorded events should already be filtered - only simultaneously occurring events on the two sides of the same module should be recorded. As, under conditions not known, single sided events are recorded as well, a software workaround is needed. All events of one side of the modules are scanned to find whether a corresponding event with the same timestamp exists on the other side. If so, a coincidentEvent is created and pushed back into the run's vector of coincident events corresponding to the module it occured in. Now, the user can decide on which modules to analyse with the setPanels() function. This can be done sequentially for multiple sets of modules without newly reading the run's data, as all the primary data is stored inside the event vector.

<div align="center">

run class members

</div>

- std::vector events

- std::vector detectorEvents

- std::vector eventsByPanels

- std::vector coincidentEvents

- std::vector selectedPanels

4.2. Search Algorithms

To analyse data, at various points searches for events with a particular timestamp have to be performed. This was simplified by the time-sorted recording of events. A first implemetation to search for coincident events was done on the base of average frequency and its standard deviation. This algorithm proved as fast and stable, though well applicable

only for two sets of timed events. That is why an advanced incremental method has been created. The number of modules is now limited only by the physically available memory and the speed is even higher.

4.2.1. Frequency Search

As this algorithm was built to run on only two sets of data, it simply walks through one set incrementally and looks for corresponding data in the other. Latter is not done in a "dumb" way by incrementing through the second set as well, but by calculating the average frequency of events inside the set and performing an intelligent guess on that basis. If the guessed event shows a different timestamp, the algorithm will keep going forward or backward in time in steps of the frequency's standard deviation until the timestamp searched for is in between two steps. Lastly, simple incrementation is used to find out whether an event at the desired point in time exists or not.

4.2.2. Incremental Search

While the frequency search increments solely one dataset, the incremental search steps through all the event tress, incrementing the one with the smallest timestamp. It then compares all events to each other, writes out the coincident ones, if any, and goes on incrementing the next smallest stamp. This assures the finding of all coincident events while keeping the speed very high.

4.3. Member Functions of the class run

Constructor run()

Whenever a new instance of "run" is created, the constructor is called. Arguments to be passed are a KaLi::KLRunIdentifier, basically a string distinctively naming the run to be analysed, such as "myo00000001", KaLi::KLDataManger, a class handling the download of the Files form IPE-servers and a toggle variable telling the constructor which data to read via the member function getRun() and what member functions to call afterwards:

Destructor run()

The destructor deletes all the contents of the vectors of events and inherited classes and clears them afterwards before deleting the member RUN which in fact frees all the memory reserved by the KaLi classes.

Toggle Choices

- **0:** Data is downloaded and both muon data and detector data are stored

- **1:** Data is downloaded and only detector data is stored

- **2:** Data is downloaded and only muon data is stored

- **3:** Data is read from local file system, only muon data is stored

getRun()

This sets the member KaLi::KLRun through the KaLi::KLDataManager and then returns its KaLi::KLRunEvents - these include all recorded events meaning also both the relevant KaLi::KLEnergyEvents and KaLi::KLVetoEvents. The getRun() function is used for example in the constructor to read the run's data.

getLocalRun()

It is not always possible to read data from the file servers, example given were files too big leading to timeouts at least in older KaLi versions. That is why the getLocalRun() function was introduced reading data from the local filesystem via the KaLi::KLRunIdentifier. The **ToDo** path to the files needs to be adapted in the source code **(environment variable?)**.

detectCoincidences()

After calling the member function channelCoincidences(), panelCoincidences(nPanels) is returned where nPanels defines, how many modules have to show coincidences for the counter to increment.

channelCoincidences()

This **always** clears the vector eventsByPanels before filling it according to the current selectedPanels settings. To do so, it loops over all entries of selectedPanels, calling loopOverSides() of the current module.

loopOverSides()

Analysing only one of the modules for coincident events between the two sides, the function runs through all the events of one panel side using the operators "<" and "==" overloaded for the class run to compare event times. For the search itself, the "A" side's index is incremented step by step while the "B" side's index is pushed up as long as its event time is smaller than A's. Every time that condition changes, it checks whether the events occured at the same time - pushing a coincidentEvent with both the events ADCValues and the timestamp into the vector for the corresponding module if so - and then going on incrementing A's index.

panelCoincidences()

As mentioned above, the first algorithm to search for coincidences between different panels was based on the average event frequency and its standard deviation, soon beeing replaced by a simpler, more efficient incremental algorithm: This features a storage for the smallest **ToDo** timestamp in a group of events. **(change code to overl.ops)** This is set to the smallest timestamp of the first event of all the modules analysed. Now, all the events are compared to the smallest one. This has the advantage, that one does not need to cross check every event with every other one but can simply compare every event to the smallest in a linear way. If simultaneous events are found, they are pushed back into the coincidentEvents vector together with the timestamp and their ADC values, nPanels is risen by one. Subsequently, the index of the smallest event storage is incremented and the new smallest event in the changed pool is searched for via the member function findSmallest(). This is repeated until all the event storages have reached their last entry. The return value is the number of events fulfilling the requirement passed through nPanels to panelCoincidences: if it is zero, every coincident event with two or more modules involved is counted, for every other number, only the number of event with exactly this number of modules is counted.

- **default/1:** Size of events returned

- **2:** Size of eventsByPanels returned

- **3:** Size of coincidentEvents returned

- **4:** Size of detectorEvents returned

findSmallest()

Setting the smallest event's timestamp through references, the findSmalles function requires only the steppoints of the different modules and returns the one with the smallest timestamp.

TOFHist()

Setting the modules to be analysed to one and two, this function was designed to analyse monitor spectrometer data. This also reflects in the fact, that both muon data and detector data are expected to be stored within the same mosxxxxxxxx run file. The function then runs channelCoincidences() and panelCoincidences() before shifting throug all the muon events searching for following detector events in a certain time interval.

TOFMuonDet()

In contrary to the TOFHist function, this one reads muon and detector data from different files as it is designed for the needs of the main spectrometer. Here, two DAQs record muon and electron detections to myoxxxxxxxx and fpdxxxxxxxx files respectively. That is why the function reads a muon run and requires a guess as to where corresponding detector data is located. It then loads on detector run after the other to check whether there's events inside a time window after each muon event. If so, a histogram is filled with the data aquired to inspect it for cumulation at particular times.

determineEfficiency

Efficiencies of modules can be determined through three of them located coextensively in front of each other. Then, all events recognised in both the uppermost and the lowest module have to - leaving geometrical inaccuracies unaccounted for - pass the middle module as well. By comparing the counts one can determine an efficiency for the module:

$$\%_{eff} = \frac{\wedge_{68}}{\wedge_{678}} \tag{4.1}$$

getSize()

The getSize() function returns the size of one of the vectors storing events or one of the inherited classes depending on the passed integer "what":

(default nonsense, reimplement)   **ToDo**

readVetoEventData(), readDetectorData() and readMOSDetectorData()

Depending on the toggle choice in the constructor, either one of the two or both of the functions are called. While the readDetectorData() function reads all recorded KaLi::-KLEnergyEvents (only the FPD records those), the readVetoEventData() function reads all the KaLi::KLVetoEvents from cards three, six and nine. This can never interfere with veto data recorded directly around the FPD vor active vetoing of detector signals, as cards 15 and 16 are used here. For analysis of monitor spectrometer data, a function

readMOSDetectorData() has been implemented reading all energy events of card one independent of channel, while of course single channels can easily be excluded. The pulser usually active at the monitor spectrometer creating KaLi::KLEnergyEvents at constant frequency is standardly excluded from analysis. All the member functions reading data require the passage of an instance of the KaLi::KLRunEvents, usually the member of the same class set in the getRun() function.4.3

5. Comissioning measurements and analysis

While the system was still under construction at the beginning of this thesis, first measurements were taken at the time with few modules under preliminary conditions to look into the behaviour of the modules. Step by step, the system was brought to completion and is now up and running. During this time, several measurements and test have been conducted to ensure the capabilities of the system meet the requirements for the KATRIN experiment. Starting at the setup of acceleration voltages, gains and thresholds, Using data obtained by the muon modules and the detector as well as other subsystems' data, the muon induced background rates and both spatial and energy distribution can be obtained. Before actual measurements, the modules had to be set up and calibrated, meaning high voltage and signal cabling needed to be installed and high voltage power supplies had to be found.

5.1. Rate instability due to charging effects

As the panels' rates were peaking over certain, short time intervals at some arbitrary frequency, it was not possible to set gains, thresholds and PMT voltages correctly as one had to be lucky to be able to identify the peak position in a calm period. It seemed there was some kind of electronic pileup. As this did not appear for all the modules it was not noticed until later into the commissioning process.

If the landau peaks were not identifiable due to prevalent electronic noise, the measurement was rendered useless as a lot of noise triggered events were recorded. As a countermeasure, in cooperation with Sascha Wuestling, potential equalisation by connecting the modules to the huge trough below the main spectrometer has been established. After the installation of the grounding, the peaking did not occur any more so the issue seems to be resolved. Now, one could make a start on setting gains, thresholds and acceleration voltages 5.2.
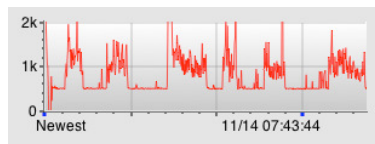

Figure 5.1.: Rate progression over the course of hours. Noticable raise in the cumulative rate of all panels in certain intervals
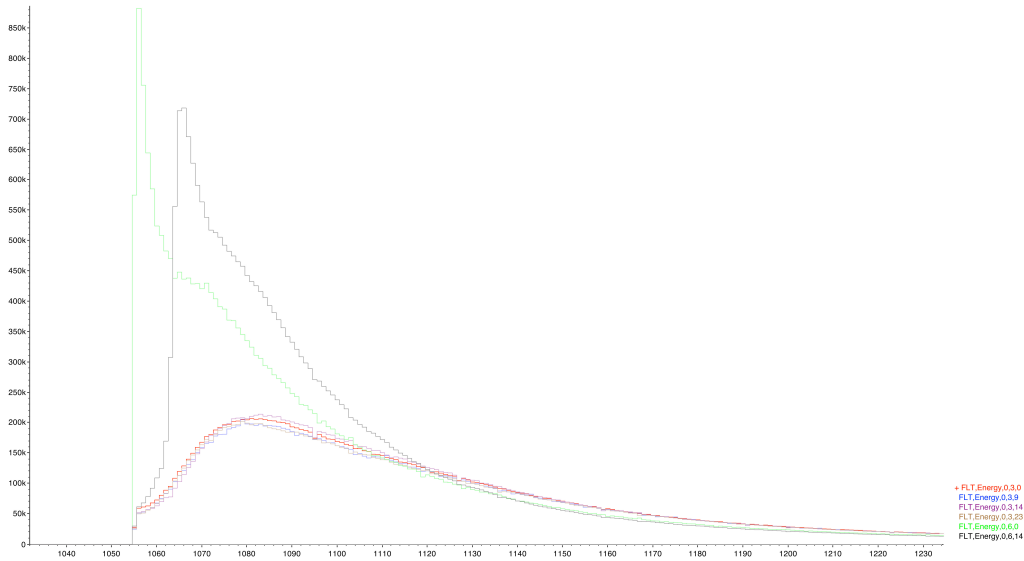
Figure 5.2.: Energy histogram of 6 channels, counts over ADC-Value. Two channels show a lot of noise around the peak position while four are developing into nice looking Landau Peaks

Figure 5.3.: Pulser shape on the left compared to actual signal shape on the right.

5.2. Gain-, Threshold and Acceleration Voltage Settings

A first amplification - linear with acceleration voltage - of the scintillation photons occurs in the photomultiplier tubes. As signals at first seemed too high for the DAQ to handle at nominal values of the datasheet, these were reduced to around 1200 V. Now, the software gains and thresholds in the ORCA software needed to be set.

5.3. Finding the best filter settings

As the PMT tubes are directly, without any preamplifiers, connected to the DAQ, the signal lengths arriving at the latter are in the order of 20 ns. This poses a problem for filters as the sampling rates need to be high and anti-aliasing is inevitable. To find the best settings, a pulser has been set up to create events at known frequency and peak heigth. The **ToDo** pulser's signal form **(what form)** was chosen as closely to the actual shape as possible, which is the "pin diode" form.

Now, to evaluate filter goodness, the width of the resulting energy histogram, which should, assuming perfect pulser signals and perfect filters, be monoenergetic, was analysed for each filter setting. This resulted in the following set of data:

On average, the boxcar filter at shaping lengths of 150 ns shows the most promising results, i.e. the sharpest peaks for any signal height. This concurs with the settings chosen for the active fpd veto; here slightly longer (around 30 ns) but comparable signals enter the DAQ, showing best results at the same filter settings[Wie13]. That is why, for any measurements **ToDo** after **(run & date)**, the new filter settings were used, bringing up the need for new threshold and gain adaptions 5.2.

5.4. Moun module's rates

A simple first check into the data is possible simply by comparing the rates measured to literature values. Here, a flux of around 1 per min and cm^2 through an area parallel to the

Panel/Side	1/A	1/B	2/A	2/B		
Card	3	3	3	3		
Channel	0	14	3	7		
PMT Voltage	1150	1150	1250	1150		
Threshold	2110	2110	2110	2110		
Gains	2350	2400	1200	2850		
Panel/Side	3/A	3/B	4/A	4/B	5/A	5/B
Card	6	6	6	6	6	6
Channel	0	14	3	7		
PMT Voltage	1150	1150	1150	1150	1150	1150
Threshold	2110	2110	2110	2110	2110	2110
Gains	2450	2400	2150	2550	2100	2400
Panel/Side	6/A	6/B	7/A	7/B	8/A	8/B
Card	9	9	9	9	9	9
Channel	0	14	3	7		
PMT Voltage	1150	1150	1150	1150	1050	1100
Threshold	2110	2110	2110	2110	2110	2110
Gains	3400	2100	2400	2500	3950	2900

Table 5.1.: **Gains, thresholds and voltages:** These are the settings that appeared to be reasonable for each panel side; furthermore, the table displays the card and channel each side is associated with in the DAQ card system

Table 5.2.: Energy resolution at different filter settings

	50 ns gap, 0 s shaping time		
	1	2	3
standard filter	1	2	3
	1	2	3
	1	2	3
	1	2	3
	1	2	3
boxcar filter	1	2	3
	1	2	3

ground is stated. Measured rates are in the order of 250 Hz. The muon modules' area is

$$315 \,\text{cm} \cdot 65 \,\text{cm} = 2.05 \,\text{m}^2 \tag{5.1}$$

Considering the 45° tilt of the modules towards the horizontal, this area reduces to an effective area of

$$A_{\text{eff}} = \sin\left(45°\right) A_{\text{real}} = 1.45 \,\text{m}^2 \tag{5.2}$$

Further taking into account detection efficiencies η discussed in 5.7, we receive an estimation of effective rate of

$$\Phi_{est} = \eta \frac{1}{\text{cm}^2 60 \,\text{s}} A_{\text{eff}} = 225 \,\text{Hz} \tag{5.3}$$

ToDo It compares well to measured rates of **(calculate actual rates)** 250 Hz.

5.5. Modules in high magnetic fields

For there is the need of moving the muon modules as close to the spectrometer tank as possible to register mostly muons that indeed went through the vessel, they are aligned closely to the air coil system. This brought up the problem of photomultiplier tubes having to work in high magnetic fields. Photomultipliers, as mentioned before, use electrons cascading in electric fields to generate amplified signals. Additional magnetic fields can keep the electrons from reaching the dynodes stopping the cascade thus keeping single events

ToDo from being registered. As rate decreases strongly under these conditions **(are there runs showing that? ask nancy)**, a solution needed to be found. As a simple, yet efficient passive counter measurement, a layer of mu-metal was wrapped around the modules. Mu-

ToDo metal is a magnetically highly permeable material (here, $\mu_r \approx$**(find out permeability)**) that guides the magnetic field lines inside itself. In doing so, the remaining flux inside a mu-metal surrounded volume, and with it the field strengths, drastically reduces. To test the improvement the mu metal coverage produces, measurements with rising aircoil currents have been performed. Steps in the size of tenths of the maximum current of mostly 100 A, in some cases only 70 A, were used to record rates over half an hour at each value. During the first run, due to a slow control problem, the current was not raised between two steps. Although displaying the expected behaviour - rates dropped much less than before - the measurement was repeated with the correct currents. Measurements show that the rate still drops at currents close to the maximum, though only to around 90 % of initial values 5.4. As, under normal measurement conditions, the coil currents are mostly around half the maximum value or less, the problem could be solved, as here, the reduction in rate is within the order errors' order.

5.6. Module Stability

If consistent factual statements on muon induced background are to be made, the modules need to work stable over the course of days, as rates are supposed to be comparable. For this reason, over the Christmas time 2012, a two-weekly measurement of half hourly runs has been taken, see 5.3 for air coil settings used. Runs myo00000051 to myo00000675 contain the data of this measurement.

The time slot was chosen for the lowly frequented spectrometer hall's sake to minimise external impacts on data taking. For analysis, a simple program to count events in variable time bins was written, creating a count histogram for all the runs in the measurement period. The result can be seen in 5.5. The observable fluctuation is well describable by fluctuations in atmospheric density, i.e. pressure and temperature, as ideally, air could be described by

$$\rho = \frac{R}{M} \frac{p}{T} \tag{5.4}$$
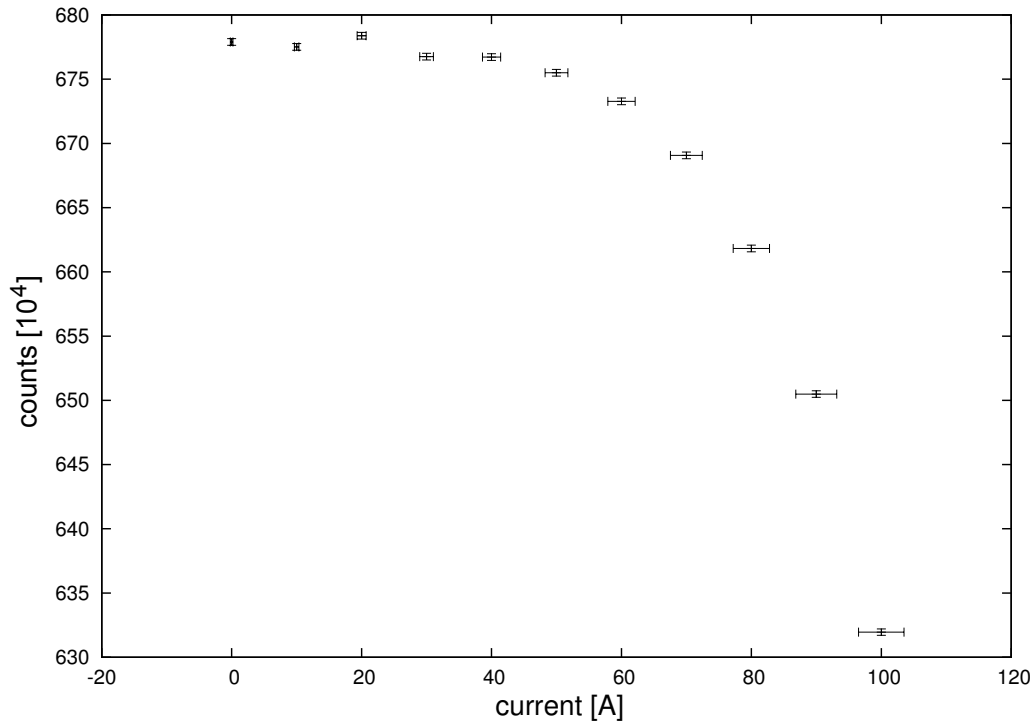
Figure 5.4.: Counts over air coil currents, with a maximum of 100 A. A clear decrease in
              rate is recognisable in the last 5 data points.

Coil #	1	2	3	4	5	6	7	EMCS h
Current [A]	10	10	14	25	42	39	54	50
Coil #	8	9	10	11	12	13	14	EMCS v
Current [A]	54	21	36	30	21	20	56	15

Table 5.3.: Runtime settings for air coils as proposed and for the comissionig measurements.
             These were kept static over the two weeks end 2012/beginning 2013

Figure 5.5.: Atmospheric density as a function of time over the course of two weeks the muon measurements took place. Note the

where ρ is the density, R is the gas constant, M is the molar mass of air and p and T are pressure and temperature respectively. If one looks at the data from **(find weather station data, see if it fits fluctuations, maybe cascade data to back it up?)**

5.7. Module Efficiency

The runs used for stability measurements, as well as any other run including modules six, seven and eight, can be used to check muon module seven for efficiency. For tests on other modules, the geometry would need to be changed so that the one to be checked is in between at least two other modules. For analysis, the function determineEfficiency() 4.3 has been written. The principle is the following: considering the small change in momentum direction high energy muons achieve through interaction with matter, one can assume straight-lined paths. From that follows, that if two parallel planes, that can be used to describe the scintillating volumes, are hit, any other, also parallel plane, in between those two will be hit as well. Keeping this in mind, one can analyse data for events registered in both modules 6 and 8 and cross check whether a event has been detected in module 7 as well. The quota of events in all three modules compared to those detected in 6 and 8 - but including the triple events - shows the efficiency of module 7. It shows that during the measurement period end of 2012, the efficiencies were at **(rerun)** 94 % which is less than one would expect at a scintillator thickness of 5 cm for muons perpendicular to the largest module surface, even more for any other. For that reason, the filter settings were checked and changed to the boxcar filter with a gap of 150 ns from the before used **(exact name)** filter. However, the expected efficiency increase was not observable, the average efficiencies before and after are within the margin of error of the other. To examine the problem further, another idea came up: modules 3, 4 and 5, that are located next to each other could be used for efficiency measurements as well considering theiy are stacked in an upright way. Using the program on those three modules resulted in even lower efficiencies of (50 ± 3) %. This raises the question wheter this is not an effect of signal filtering, but a previously not considered physics effect. One thing comming to mind is deviation of the muon track from linear forms. This feature would comply with the seemingly lower efficiency at the upright stacked modules, where, at equal bending radii, the ratio of muons travelling around the middle module is higher due to the lower total area in stacking direction. This thesis should be tested. This can be done both by simulating the cosmic muons including magentic fields and empirically by varying the distance between teh single modules. The latter is difficult not only because the modules are heavy and not made for lifting (no designated carrying structures), but also because movement always means potential danger to the photomultiplier tubes and their connection to the scintillators. Furthermore, if all coils and solenoids were to be turned of simultaneously at some point, one could collect data then and see how efficicencies change during that (there have been runs taken when that was still the case, but only few modules were working properly at that point). If the dependence on module distance turns out to be true, but the efficiencies are still below expected values at the lowest possible distances, a possible improvement would be to use preamplifiers before signals arrive at the DAQ. These would widen the signals timewise leading to a more easily detectable signal for the filters.

5.8. Photo Multiplier Tube Test with Sr source

With sets of four photomultiplier tubes being read out over one cable, and, consequently, via one channel, the test of individual PMTs is not trivial. Nevertheless, a method using

a simple graph
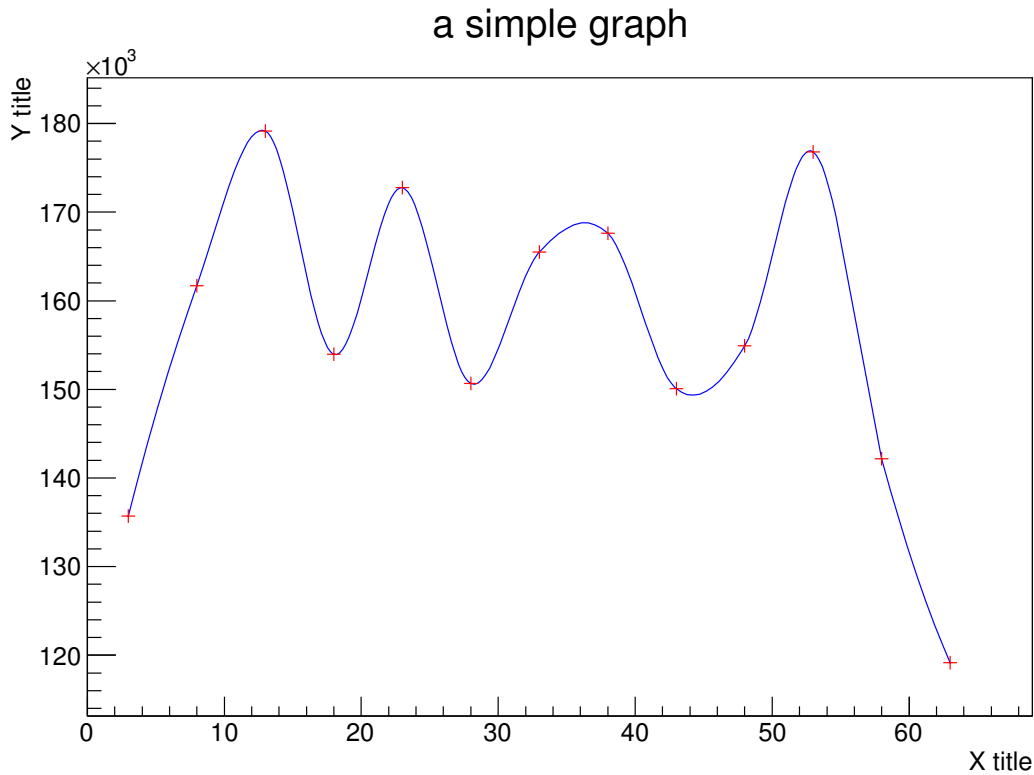
a MBq ^{90}Sr source to trigger events was used to check functionality. Of course, all tubes were able to see the source at any position but rates were expected to rise as the distance to any of the tubes shrank. A source holder was constructed from acrylic glass to shield the user from radiation and to attach the source to the modules, as a large dependence of rate on the position was found when the source was simply duct taped to the modules. As the foil mantling of the modules absorbs a non negligible part of the radiation emitted from the source, it had to be ensured that the number of layers was equal for all measurements. This was given only below the modules as the foil has been folded around them at the ends in a gift wrapping way. Thus, the source was pretty far away from the photomultiplier tubes making it more difficult to distinguish between them. A first measurement was then to check for exactly that distinguishability.**(insert measurement for small steps over PMTs positions)**.   **ToDo**

As one can see a rise in rate at the positions the tubes are located at, it was decided that four measurements per module and side were sufficient, especially as all measurements can afterwards be compared to each other. The tube positions at **(n,n,n,n cm)** were used as **ToDo** measurement positions as well. For each side, a run has been taken containing five minute subruns for every position. Figure 5.7 shows the result of these measurements. One can see that the gerneral shape of each side compares very well to the others. Exceptions are **(which ones different?)**showing slight, but acceptable deviations off the norm.   **ToDo**

5.9. Synchronisation of moun module and FPD DAQs

Measuring time differences on a μs scale requires exact synchronisation of the two differen DAQs used for data acquisition. For this purpose, a clock has been designed sending signals at two frequencies: one at $1\,\mathrm{Hz}$ and one at $10 \times 10^6\,\mathrm{Hz}$ internally converted to a $20 \times 10^6\,\mathrm{Hz}$ signal by the DAQ. Those signals can be synchronised to the timestamps of GPS satellites if a GPS antenna is connected. This has not yet been done as relative synchronization between the two crates is sufficient for the purposes of finding correlations between muon and detector events. As the cable length for signal transmission is pretty extensive - around
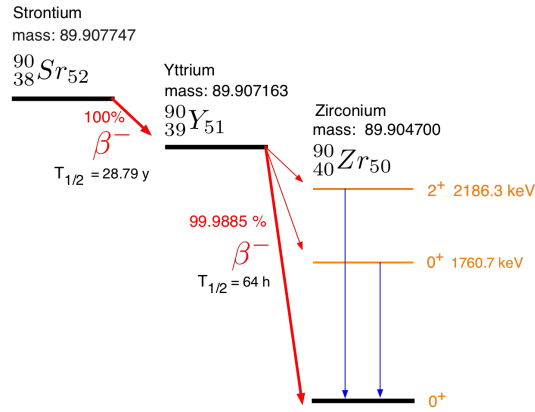
Figure 5.6.: Decay mechanism of ^{90}Sr: first a lower ernergetic decay to ^{90}Y emitting 544 keV/c^2 electrons, from that most probably a higher energetic decay to ^{90}Zr ground state (2.29 MeV/c^2 electrons) or, with low probabilty, to one of two of its excited states.
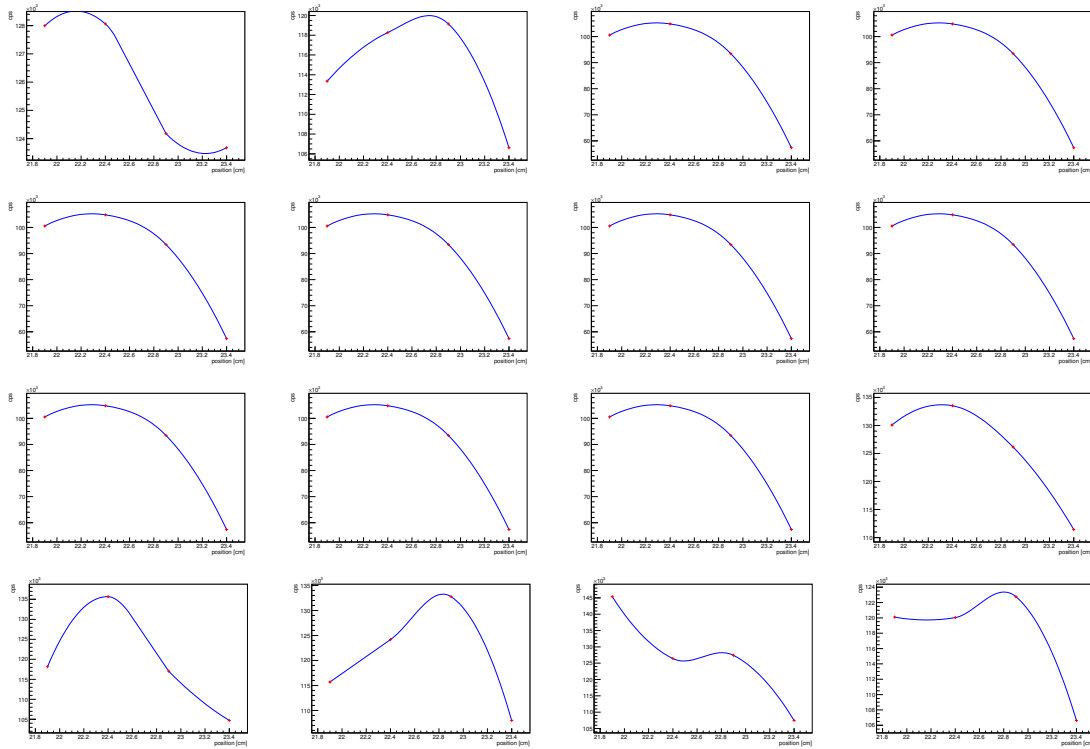

Figure 5.7.: Measurements with source at different positions

Figure 5.8.: Subsecond time differences before firmware update: Large differences between the events,

50 m - it was decided to use optical fibers instead of CAT 5 cabling. As two signals need to be transmitted, paired **(connection type name)** fibers were used. The clock itself has optical outputs, the DAQ though needs converters from optical to electrical signals and a modified SLT back panel card to receive the converted signals via Cat 5 cable. **ToDo**

To test the setup, the muon DAQ was moved to the detector platform. Both crates were fed by a pulser signal. Runs at different frequencies were recorded to test both the synchronisation and the detection of events. To synchronize timestamps to an external signal, the FLT cards drop down menu needs to be set to **(look up)** and the SLT needs to be set to **(lookup too)**. At first, manually triggered signals were used in minute runs to check the timestamps equality. Several runs were taken, all showing that the events were shifted by several µs **ToDo** **ToDo**

In close cooperation with the IPE it was found that this was merely a problem of firmware versioning as well as software settings in Orca resolving the problem quickly. After installing the latest firmware, more runs were taken now displaying the desired behaviour: Following the manually triggered events, runs with fixed frequency events were recorded, raising the frequency to up to **(find maximum)**. All the test worked fine including starting one DAQ's run way ahead of the other. Those events recorded in both run files were always well synchronized. Afterwards, the muon DAQ was moved back to its original position and the optical fibers were stowed in wire-ways guiding it from the detector platform down to the basement where the muon detection system is located. Another problem occurred here, as signal transmission was impaired by a kink at one of the turns, but was quickly resolved by smooth rewiring. Concluding, it can be said that the clock runs continuously without any problems throughout all the measurements - including main spectrometer commissioning measurements. **ToDo**

5.10. Coincidence Search between Muon- and Detector Events

If one wants to actually detect background induced by myonic events registered by the muon modules, those events need to be correlated to detector events time wise. For this purpose, the analysis code's class run was extended by the member functions TOFHist()4.3 and TOFMuonDet()4.3, where the former is used for monitor spectrometer analysis and the latter for the main spectrometer. The biggest difference is that, at the main spectrometer, two DAQs leading to runs with different starting times and of different lengths are created that need to be compared.

5.10.1. Monitor Spectrometer

Measurements at the monitor spectrometer are easily manageable due to the fast accessibility of all the components and the collection of data in a single run file through the mini crate. For measurements, high voltage supplies have been added to the **(name of the rack)** rack and the readout electronics were connected to a second FLT-card inserted into the **ToDo**

Figure 5.9.: Time differences between events after firmware upgrades. Differences between the event times are within one 50 ns bin

asymmetric magnetic field

Run	solenoid source	solenoid detector	inner aircoil	outer central aircoil	outer aircoil	emcs x	emcs y
mos00159395	0	25	0	-4	-4	2	-19.5
mos00159396-mos00159398	0	50	0	-8	-8	2	-19.5
mos00159399	0	50	0	-7	-7	2	-19.5
mos00159400	0	50	0	-6	-6	2	-19.5
mos00159401	0	10	0	-2	-2	2	-19.5

non-axially symmetric magnetic field

Run	solenoid source	solenoid detector	inner aircoil	outer central aircoil	outer aircoil	emcs x	emcs y
mos00159753-mos00159753	25	25	7	7	5	0	-14
mos00159753-mos00159753	25	25	7	7	5	0	-14

Figure 5.10.: Flux tube at asymmetric magnetic fields. Electrons from processes at the walls are guided directly towards the detector as the largest part of the flux tubes surface ends in the monitor spectrometer's vessel's wall

mini DAQ and operated in veto mode. Gains and thresholds were easily set as only four sides had to be adjusted - compared to the 16 main spectrometer channels. The PMT tubes were operated at $1.5\,\mathrm{kV}$. The detector gain and threshold settings for the 5 pixel detector have been kept, although the detector position has been shifted to the position at which the center pixel exhibited maximum rate and the pairs of east-west and top-bottom pixels showed comparable count rates. Furthermore, the recording mode was switched from histogram mode to energy mode as the timestamps for every single event were needed for analysis. Several hourly runs have been taken under different magnetic field compositions. Both asymmetric magnetic 5.10 and non-axially-symmetric field 5.11configurations have been investigated: **()** The TOFHist4.3 function has been used to analyse the data. It browses through all the muon events detected and finds any detector event in a definable timespan after the muon event. This can be more than one detector event per muon event. In all of the settings, a clear peak is visible at around $7\,\mathrm{\mu s}$. As for count rates, they are a lot higher in the asymmetric magnetic field setup as secondary electrons are guided from their point of origin to the detector instead of mostly being magnetically shielded. In this setup, only the reflection through the rise in magnetic field on the electrons' paths takes its toll on the rate. The exact values are: **(Do analysis for every measurement, insert peak positions + stdev)**

ToDo

ToDo

5.10.2. Main Spectrometer

Monitor spectrometer results suggested that the time of flight was well measurable, even if on bigger scale, at the main spectrometer. So, during commissioning measurements, already parallel to measurement M1, sone runs with asymmetric magnetic field have been

Figure 5.11.: Flux tube at non axially symmetric fields. Although no direct guidance from the wall to the detector is given (the flux tube never touches the wall in this configuration), by adding a magnetic component perpendicular to z-direction, the probability for entrance into the flux tube rises strongly.

Figure 5.12.: Time difference histogram for asymmetric magnetic fields.

Figure 5.13.: Flux tube at non axially symmetric fields. Although no direct guidance from the wall to the detector is given (the flux tube never touches the wall in this configuration), by adding a magnetic component perpendicular to z-direction, the probability for entrance into the flux tube rises strongly.

taken with switched polarity or turned off pre spectrometer magnets compared to standard setup. The data was analysed for each single ring of the FPD. Search parameters were the time slot from $0\,\mathrm{s}$ to $15\,\mathrm{\mu s}$ though remains inconclusive at the moment, see 5.14. Analysis for every single pixel was not possible due to much too low statistics, though it might be more conclusive as less different paths contibute to the single pixel. On the other hand, after the non-central alignment of the detetor has been fixed using different settings for the LFCS-system, under asymmetric magnetic fields, the fields should be rotationally symmetric around the z axis disregarding small deviations. Assuming this, the path lengths for every pixel of one ring should be very comparable.

The failure to find a clear runtime for electrons induced by muonic events might be due to the combination of muon module position and the magnetic field setup as the wall area covered by the flux tubes and the volume surveilled by the muon modules did not overlap very much. Furthermore, due to the very low magnetic field at the wall compared to the volume inside the detector and pinch magnet, most of the induced electrons are magnetically reflected as the maximum polar angle towards magnetic field lines θ_{max} is defined by

$$\frac{B_{min}}{B_{max}} \approx \frac{3\,\mathrm{G}}{4\,\mathrm{T}} = sin(\theta_{max}) \tag{5.5}$$

meaning only angles satisfying the inequation

$$\theta < \arcsin \frac{B_{min}}{B_{max}} = \arcsin \frac{3\,\mathrm{G}}{4\,\mathrm{T}} = 0.004° \tag{5.6}$$

will be able to reach the detector. All others will be reflected and fly back to the wall to be absorbed in the conducting wall material. **(set real field values)** As a result, compared **ToDo** to the monitor spectrometer, where the ratio is a lot greater, less of the muon induced electrons arrive at the detector making long measurements a requirement for good statistics. This leads to detector rates of only around $2\,\mathrm{cps}$, depending on the inner electrode voltages. At high inner electrode voltages, the rate increases strongly to $150\,\mathrm{cps}$ which is probably due to field emission from the electrodes. These measurements should be repeated when high voltage can be applied to the main vessel.

Following that presumption, for M6 measurements, the setup was changed. The fluxtube was widened for its outer parts to hit the spectrometer wall in regions around combs n and n **(which combs)**. This raises the probability of the muons detected being those **ToDo** inducing secondary electrons at the vessel as well. Also, the LFCS setup was changed in such fashion that the magnetic field at the spectrometer wall is higer by a factor of two, directly resulting in a higher angular acceptance of electrons. The resulting flux tube is shown in figure 5.17. **(flux tube including modules for horizontal and vertical** **ToDo** **view) (If data will be taken add to analysis.)** **ToDo**
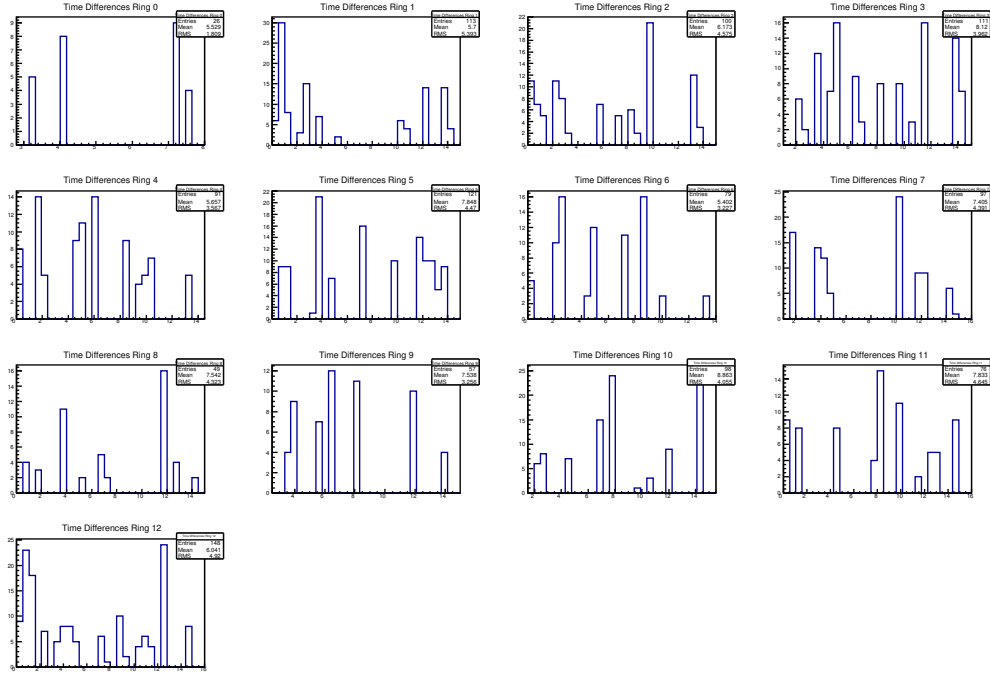
Figure 5.14.: Time differences of muon events followed by a detector event. From left to
right and top down for every single detector ring, 0 being the innermost and
12 being the outermost ring.

Figure 5.15.: Flux tube in field configuration M12.8

Figure 5.16.: Rate trend over inner electrode voltages

Figure 5.17.: new flux tube

6. Simulation of muon induced background

To compare the data aquired to theoretically expected values, a Geant4 simulation of cosmic showers has been set up including the geometry of the main spectrometer as well as the muon modules. Using this software, any number of inciding muons can be simulated and the effect on the main spectrometer and the muon modules can be evaluated.

6.1. Geant4

The Geant4 package is a powerful tool for simulation of particles. It has loads of possible interactions already integrated making it easy for the user to set up and run simulations. After setting up geometry and detectors, the user starts a run. Each run may consist of one or more events. During a single run, a loop of processes is called:

- Primary Generator Action

- Run action

- Event action

- Stacking action

- Tracking action

- Stepping action

For user interaction, for each item above, classes with the addition 'user' to the base classes name can be called before or after the standard action class. An example is the class G4UserEventAction invoked before and after each call of G4TrackingAction. It contains two member classes, namely BeginOfEventAction and EndOfEventAction that let the user decide what to do at this point. Through those, it is possible to change behaviour of the simulation or extract data needed. In this case, for every event, if more than one module has been hit, the copy numbers of those are pushed back to a vector of event data. Running the simulation, one can either interactively enter commands or write those to a .mac file, by default the vis.mac file, which are then sequentially executed.

Figure 6.1.: Dependance of muon rate on zenith angle.

6.2. Geometry setup

To set up a geometry, the class G4VUserDetectorConstruction is used. B1DetectorConstruction inherits from that as a base class and additionally contains all of the geometrical parameters needed for the setup such as radii of the main spectrometer cones or positions and extent of the muon modules. Every shape generated is made up of both a logical volume G4LogicalVolume and a physical volume G4PhysicalVolume. The logical volume describes the intrinsic properties of the geometric obect added: its shape, its size and its material. The physical volume accepts a logical volum as input providing position and alignment of the previously defined. Inside the detector construction class, all of the materials used in the simulation need to be defined as well. These are the components of the air outside and inside the spectometer including pressures and constitution, the stainless steel of the spectrometer wall and the scintillator material of the muon modules. The main spectrome-

ToDo ter geometry was already **(written by who?)** existant but had to be modified as many border volumes were implemented. These were very flat volumes covering any area of the main spectrometer not needed for this simulation. Additionally, the muon modules have been added as sensitive volume. Keeping in mind that one wants to not only distinguish wheter a module has been hit, but also which one. That is why the logical volume for every module is the same wheras the physical volume is a copy of the first at different world coordinates making them identifiable via their individual copy number.

6.3. Muon generator

Muon generation was realised through the primary generator action. The angular distribution suggested by Henrik Arlinghaus [Arl09] was implemented. The angular rate

ToDo dependance is shown in 6.1.The energy was set to **(reasonable value)** disregarding the actual anergy distribution as this was mainly about flight paths that are not strongly dependant on energy at high energies. Starting positions were spherically distributed, with the direction towards the origin, which is in the center of the main spectrometer. Positions were then randomly moved in a volume surrounding the spectrometer to account for the non-point like structure of the detection system as a whole, while the distribution describes a single point in space.

6.4. Hit counter

For comparing the simulation to real data, of all the events generated, those hitting modules were counted. Each event containing at least one hit is written into a file for further analysis. This made it possible to compare the rates of the single modules, showning that the generator works fine. furthermore, it allowed for a estimation of muons hitting the modules compared to the total of inciding muons.

7. Conclusion

8. Outlook

...

Bibliography

[Abe13]   K. e. a. Abe, "Evidence for the appearance of atmospheric tau neutrinos in super-kamiokande," *Phys. Rev. Lett.*, vol. 110, p. 181802, May 2013. [Online]. Available: http://link.aps.org/doi/10.1103/PhysRevLett.110.181802

[Arl09]   H. Arlinghaus, "Investigation of the muon-induced secondary electron background in the katrin experiment," http://www.uni-muenster.de/Physik.KP/ AGWeinheimer/Files/theses/Diplom_Henrik_Arlinghaus.pdf, 2009, [Online; accessed 21-08-2013].

[asd12]   asdf, "Neutino mass hierarchy," http://scienceblogs.com/startswithabang/files/ 2012/01/mass-hierarchy.jpg, 2012, [Online; accessed 21-08-2013].

[BKR09]   S. Becker, H. Koziolek, and R. Reussner, "The Palladio component model for model-driven performance prediction," *JSS*, vol. 82, pp. 3–22, 2009. [Online]. Available: http://dx.doi.org/10.1016/j.jss.2008.03.066

[Cry05]   S.-G. Crystals, "Premium plastic scintillators," http://www.detectors. saint-gobain.com/uploadedFiles/SGdetectors/Documents/Product_Data_ Sheets/BC400-404-408-412-416-Data-Sheet.pdf, 2005, [Online; accessed 11-07-2013].

[DHMW13] G. Drexlin, V. Hannen, S. Mertens, and C. Weinheimer, "Current Direct Neutrino Mass Experiments," *ArXiv e-prints*, Jun. 2013. [Online]. Available: http://arxiv.org/abs/1307.0101

[Sta04]   T. Stanev, *High Energy Cosmic Rays*, 2004.

[Wie13]   K. Wierman, personal conversation, 2013.

Appendix

A. First Appendix Section

ein Bild

Figure A.1.: A figure

. . .